Trinh, Xuan-Long; Kim, Hyun-Chul

Article

Fully solution-processed perovskite solar cells fabricated by lamination process with silver nanoparticle film as top electrode

Energy Reports

Provided in Cooperation with:
Elsevier

Suggested Citation: Trinh, Xuan-Long; Kim, Hyun-Chul (2020) : Fully solution-processed perovskite solar cells fabricated by lamination process with silver nanoparticle film as top electrode, Energy Reports, ISSN 2352-4847, Elsevier, Amsterdam, Vol. 6, pp. 1297-1303, https://doi.org/10.1016/j.egyr.2020.04.037

This Version is available at:
https://hdl.handle.net/10419/244121

Energy Reports 6 (2020) 1297–1303

Contents lists available at ScienceDirect

Energy Reports

journal homepage: www.elsevier.com/locate/egyr

Research paper

Fully solution-processed perovskite solar cells fabricated by lamination process with silver nanoparticle film as top electrode

Xuan-Long Trinh, Hyun-Chul Kim *

High Safety Vehicle Core Technology Research Center, Department of Mechanical and Automotive Engineering, Inje University, 197 Inje-ro, Gimhae-si, Gyeongsangnam-do 621-749, South Korea

ARTICLE INFO

Article history:
Received 11 October 2019
Received in revised form 26 March 2020
Accepted 29 April 2020
Available online xxxx

Keywords:
Perovskite solar cells
Lamination process
Silver nanoparticle film
Solution process
Spin-coating

ABSTRACT

Perovskite solar cell is one of the most promising candidates for future photovoltaic market because of its high power conversion efficiency (>25%). However, most metal top electrodes are typically fabricated by a vacuum deposition method, which makes the fabrication expensive and unsuitable for commercial applications. In this paper, we present devices in which every layer was prepared using a solution process, with a laminated silver nanoparticle film serving as the top electrode. The silver nanoparticle film was produced by spin-coating the nanoparticle silver ink onto a poly(ethylene terephthalate) (PET) substrate followed by post-annealing at 150 °C for 5 min. Introduction of a thin layer of Poly(3,4-ethylenedioxythiophene) polystyrene sulfonate (PEDOT:PSS)/D-sorbitol, plays an important role in improving the adherence of devices and electrical contact during lamination. Thereby, laminated perovskite solar cells with average power conversion efficiency (PCE) of 10.03% were achieved, almost of 90% of the PCE obtained for conventional devices (11.19%) with evaporated silver contact. The electrical and morphological properties of thermally annealed silver nanoparticle film were also investigated.

1. Introduction

Although organic–inorganic lead halide perovskite solar cells (PSCs) exhibit certain limitations, such as short-term device stability (Frost et al., 2014; Stranks and Snaith, 2015), anomalous J-V hysteresis (Snaith et al., 2014), and environmental impacts because of the appearance of lead compounds (Yoo et al., 2019), they surpass commercial solar cell as promising candidates in photovoltaic technologies. The PSCs were first introduced in 2009 by Kojima et al. (2009) who used a perovskite material as a visible-light sensitizer in dye-sensitized solar cells with PCE of 3.8%. These solar cells had very low efficiency because of the dissolution of perovskite in the electrolyte and were not attractive until a new solid-state mesoscopic perovskite solar cell was reported in 2012 by Kim et al. (2012a). In that study, they fabricated a perovskite solar cell using methyl ammonium lead iodide (CH_3NH_3)PbI_3 perovskite nanocrystals as the light absorber and Spiro-MeOTAD as a hole transport layer to improve its PCE (9.7%) and stability (over 500 h) without encapsulation. Since then, extensive research in PSCs has been devoted to the development of device architecture (Ball et al., 2013; Liu and Kelly, 2013), morphological control of perovskite layer (Burschka et al., 2013; Kim et al., 2014), and hole-transport layer engineering (Chen et al., 2019; Schloemer et al., 2019) and hence led to a significant increase of PCE (>25%) (Best Research-Cell Efficiency Chart | Photovoltaic Research | NREL, n.d., 0000). The PSCs are interesting due to their high PCE and wide range of fabrication techniques from solution to vacuum processing (Song et al., 2016). In addition, the architecture of PSCs is very diverse, which is an advantage in both scientific and industrial researches.

The PSCs with high PCE are generally produced utilizing thin a metal film (typically Au, Ag, or Al) as the top electrode. These metal electrodes are deposited directly onto the active materials by vacuum deposition method and act as an effective ohmic contact. The available deposition methods are expensive and time-consuming and hence not suitable large-area PSCs and industrial manufacturing. The lamination process is an excellent alternative to replace vacuum deposition method due to its low cost, ease of processing, and potential to scale-up. In 1988, Granstrom et al. initiated the lamination process followed by the controlled annealing to produce two-layer diodes (Granström et al., 1998). The process is now frequently employed to fabricate solar cells, especially on semi-transparent devices (Bryant et al., 2014; Gaynor et al., 2010; Huang et al., 2008; Makha et al., 2016). In this process, the device is separated into two parts: bottom part and top part. The bottom part consists of an active layer and is fabricated by conventional methodologies. The top part contains a metal counter electrode and is coated by solution-based

* Corresponding author.
E-mail address: mechkhc@inje.ac.kr (H.-C. Kim).

https://doi.org/10.1016/j.egyr.2020.04.037

methods on another substrate. They are then laminated with a gentle external force. To couple the two parts together, a mixture of PEDOT:PSS/D-sorbitol has been widely utilized as a conductive glue layer. Ouyang et al. introduced this material in 2006 to produce a polymer light-emitting diode by lamination process (Ouyang and Yang, 2006). The physical properties of PEDOT:PSS/D-sorbitol were further investigated and improved to make it suitable for solar cell fabrication (Makha et al., 2016; Shimada and Shiratori, 2013). Shimada et al. reported the effect of D-sorbitol content on the work function, viscosity, surface tension, and conductivity in conductive glue layer, and then optimized it for photovoltaics (Shimada and Shiratori, 2013).

The lamination process has been employed for fabricating a wide variety of top electrode materials, such as ITO (Huang et al., 2008), carbon nanotube (Kim et al., 2012b), graphene (You et al., 2015), PEDOT:PSS (Bu et al., 2015; Yin et al., 2014), and metal nanowires (MeNWs) (Ag, Cu, and Ni) (Bryant et al., 2014; Guo et al., 2015; Hwang et al., 2016). Among them, the AgNWs mesh electrode is the most commonly used in photovoltaic devices because of its high optical transparency and low sheet resistance. In addition, AgNWs mesh electrode can be easily formed on various substrates by using solution-based deposition methods, including doctor blading, spin-coating, and spray-coating. Makha et al. initiated the fabrication of PCSs with laminated AgNWs mesh as a top electrode (Makha et al., 2016). The cell structure was FTO/compact TiO_2/mesoporous TiO_2/perovskite/Spiro-MeOTAD/PEDOT:PSS/D-sorbitol/AgNWs mesh and its PCE was stabilized at (7.6 $\pm$ 1)%, corresponding to 80% of the PCE of opaque gold electrode. However, Khaligh et al. indicated that AgNWs mesh electrode can fail because of Joule heating during device operation, which causes AgNWs to breakup and thus form an electrical discontinuity in the NWs film (Khaligh and Goldthorpe, 2013). In addition, AgNWs mesh electrode restricts the light reflection back into the active layer, thereby degrading PCE of the PSCs.

Prior to the development of above materials, nanoparticle silver inks have been widely used to create patterns on any substrates in printing technology owing to ease of processing, high electrical conductivity, and stability. Usually, nanoparticle silver inks are sintered to establish contact between the particles and evaporate the solvent after they have been printed on a suitable substrate. The process of sintering and solvent evaporation limit the applications of nanoparticle silver inks in PSCs because this process can adversely affect sensitive components inside the photovoltaic devices. This problem can be completely eliminated using the suggested lamination process. Greer et al. reported that the resistivity of silver conducting film produced from spin-coated nanoparticle silver inks approaches to that of bulk silver at 150 °C (Greer and Street, 2007). This silver nanoparticle film is area suitable replacement for evaporated metal electrode in PSCs. However, limited literature is available about the use of silver nanoparticle film to fabricate PSCs.

Therefore, we report a fully solution-processed fabrication of perovskite solar cell using silver nanoparticle film as the top electrode by lamination. The configuration of perovskite solar cell is FTO/compact TiO_2/mesoporous TiO_2/$CH_3NH_3PbI_3$/Spiro-MeOTAD/PEDOT:PSS/D-sorbitol/silver nanoparticle film. The silver nanoparticle film is formed by spin-coating the nanoparticle silver inks on PET substrate followed by annealing on hot plate. During this process, heating temperature is investigated to optimize the sheet resistance and surface roughness of annealed silver nanoparticle film. Perovskite solar cells were fabricated under a relative humidity of ~45% with stabilized PCE of 10.03%.

2. Materials and methods

2.1. Methyl ammonium iodide (CH_3NH_3I) synthesis

High-purity chemicals were bought from commercial companies and were used as received. The CH_3NH_3I was prepared according to the reported procedure (Kim et al., 2012a). A 27.8 mL of methylamine (40 wt% in methanol, TCI) was mixed with 30 mL of hydroiodic acid (57 wt% in water, Aldrich) under vigorous stirring for 2 h in an ice bath. The resulting solution was evaporated at 50 °C for 1 h to gain the precipitated CH_3NH_3I. This precipitate was washed several times with diethyl ether and finally dried under vacuum overnight. The final product was used without further purification.

2.2. Solar cell fabrication

Solar cells were fabricated under indoor ambient conditions. The room temperature and relative humidity were mostly about 28 °C and 45%, respectively. Fluorine-doped tin oxide (FTO) glasses (7 Ω/sq, 1.5 × 1.5 cm^2) were cleaned in an ultrasonic bath with deionized water, acetone, and isopropanol for 10 min each. The substrates were then treated in a UV-ozone cleaner for 15 min. For the formation of a compact TiO_2 (cp- TiO_2) layer, a 0.15 M solution of titanium diisopropoxide bis(acetylacetonate) (75 wt% in isopropanol, Aldrich) in 1-butanol (99.8%, Aldrich) was spin-coated on cleaned FTO substrate at 2000 rpm for 30 s. The wet film was then heated at 125 °C for 5 min. After cooling to room temperature, a diluted TiO_2 paste (Solaronix, T/SP: ethanol = 1:3 by weight) was spin-coated on the compact TiO_2 layer at 3500 rpm for 20 s and immediately dried at 125 °C for 5 min. The film was annealed at 450 °C for 30 min to form a mesoporous TiO_2 (mp- TiO_2) film. The resulting mp- TiO_2 layer was then doped with lithium (a 0.1 M solution of bis(trifluoromethane) sulfonamide lithium salt in acetonitrile) (Giordano et al., 2016). This solution was dropped on the substrate with 5 s loading time and then spin-coated with an acceleration of 1000 rpm s^{-1} to a final speed of 3000 rpm for 30 s. The substrate was again heated at 450 °C for 30 min.

The perovskite layer was formed on top of mp- TiO_2 using two-step spin-coating procedure. PbI_2 solution (1 M) was prepared by dissolving 462 mg PbI_2 (99%, Aldrich) in 1 mL N,N-dimethylformamide (DMF, 99.8%, Aldrich) under stirring at 70 °C. 100 μL of PbI_2 solution was spin-coated on the mesoporous TiO_2 at 4000 rpm for 20 s, and the film was then dried on a hot plate at 40 °C for 5 min, followed by 100 °C for 5 min. After cooling to room temperature, 200 μL of 0.063 M (10 mg/mL) CH_3NH_3I solution in isopropanol was loaded on the PbI_2 layer for 60 s (loading time) and then spin-coated at 4000 rpm for 20 s. The film was immediately dried at 100 °C for 5 min.

The hole transport material (HTM) 2,2′,7,7′-tetrakis(N,N-di-p-methoxyphenylamine)-9,9-spirobifluorene (Spiro-MeOTAD) solution was prepared by dissolving 72.3 mg of Spiro-MeOTAD in 1 mL of chlorobenzene, to which 28.8 μL of 4-tert-butyl pyridine and 17.5 μL of lithium bis(trifluoromethanesulfonyl)imide (Li-TFSI) solution (520 mg Li-TSFI in 1 mL acetonitrile, Sigma-Aldrich, 99.8%) were added (Im et al., 2014). 40 μL of sprio-MeOTAD was spin-coated on the perovskite layer at 2000 rpm for 30 s.

The perovskite solar cells were finished by covering the top electrode on the HTM. For the lamination process, PET substrates were wiped with acetone and then sonicated in isopropanol for 10 min. A 100 μL of nanoparticle silver inks was spin-coated on cleaned PET substrate at 2000 rpm for 30 s, which was immediately heated on a hot plate at 150 °C for 5 min to gain the smooth silver layer. A 100 μL of PEDOT:PSS/D-sorbitol solution was spin-coated on the silver layer at 1000 rpm for 60 s. The

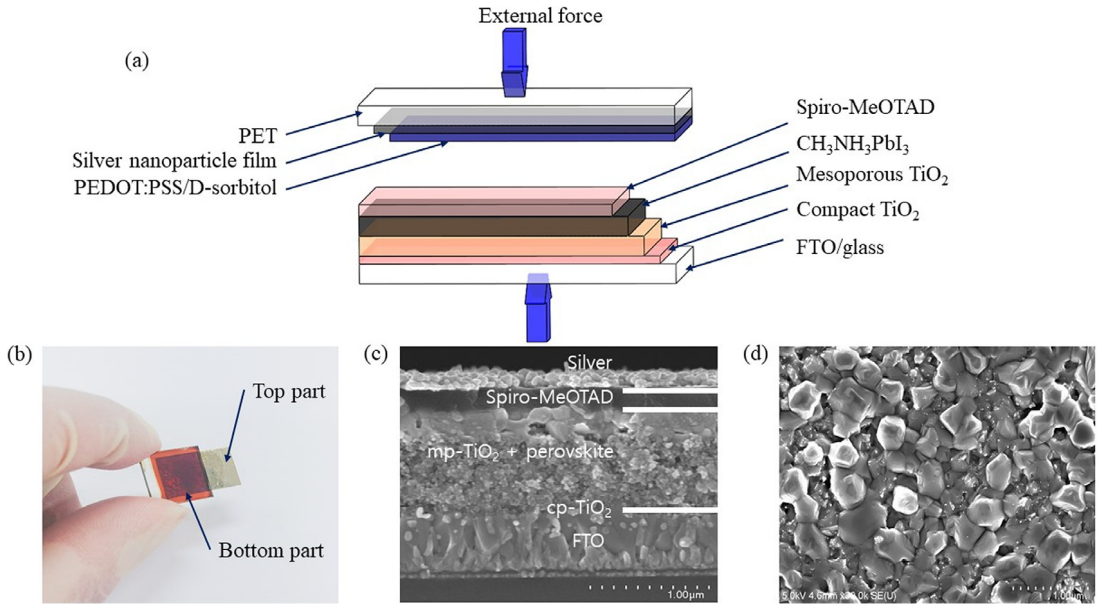

Fig. 1. (a) A schematic illustration of lamination process for PSCs fabrication, (b) laminated cell, (c) cross-section image of conventional PSCs, and (d) top-view SEM image of perovskite layer.

PEDOT:PSS/D-sorbitol solution was prepared by dissolving the 400 mg D-sorbitol (98%, Aldrich) in 1 mL PEDOT:PSS (PH 1000, Ossila) dispersion under stirring overnight (Makha et al., 2016). This solution was the filtered by syringe filter (0.45 μm of pore size). The PET/silver nanoparticle film/PEDOT:PSS/D-sorbitol electrode was then heated at 120 °C for 10 min and immediately laminated on the HTM layer using finger pressure. The contact area between two parts of cell was typically 1 × 1 cm^2. For the comparison, Ag electrode was thermally evaporated at 2.5 Å s^{-1} on the same HTM.

2.3. Characterization

The photocurrent density and voltage curves were measured using a PEC-L01 portable solar simulator (Peccell) with an AM 1.5G filter on the day of fabrication. The cells were scanned at a scan rate of 0.1 V s^{-1}. While measuring the current and voltage, the laminated cells were covered with a black mask aperture of diameter 5 cm to determine the active area. For the Ag evaporated cells, the active area was defined by the size of the silver electrode (0.14 cm^2). The top-view surface and sheet resistance of silver nanoparticle film were measured using a scanning electron microscope (SEM, Hitachi S-4800) and a four-point probe method (NI cDAQ-9178), respectively.

3. Results and discussion

Fig. 1(a) shows a graphical illustration of the lamination process for the fabrication of perovskite solar cell. The working principle is similar to that of conventional perovskite solar cell. The incident light is illuminated through the FTO glass and absorbed by perovskite layer to generate charge carriers. The electrons and holes are collected by the TiO_2 and HTM Spiro-MeOTAD layers, respectively. The PEDOT:PSS/D-sorbitol layer was used as the conductive adhesive to improve the electrical contact between the HTM Spiro-MeOTAD and the silver nanoparticle film. The fully solution-processed laminated device was fabricated in two parts: bottom part and top part. The bottom part consisted of an FTO layer on glass substrate, a ∼40-nm-thick cp-TiO_2 layer, a ∼650-nm-thick mp-TiO_2, a ∼300-nm-thick perovskite layer, and a ∼200-nm-thick HTM Spiro-MeOTAD layer. The top part included a ∼120-nm-thick silver nanoparticle film on a PET substrate and a ∼1000-nm-thick layer of PEDOT:PSS/D-sorbitol. An example of laminated cell is showed in Fig. 1(b). For conventional devices, the top part of laminated device was replaced by a ∼110-nm-thick silver layer, which was formed by thermal evaporator, as shown in Fig. 1(c). The perovskite layer was fabricated on the mp-TiO_2 layer by a two-step spin-coating procedure, without using any solvent engineering treatment methods. Its top-view SEM image (Fig. 1(d)) indicates that surface is fully covered with perovskite with average grain size of 300 nm.

The nanoparticle silver inks consist of a mean particle size of ∼20 nm in an organic solvent. The nanoparticle silver inks can be easily spin-coated on a PET substrate and converted into a silver nanoparticle film through annealing on a hot plate. This phase transport process takes place in two stages: solvent evaporation stage and atomic diffusion stage driven by the reduction of interfacial energy (Greer and Street, 2007). To investigate the effect of annealing temperature on the electrical and morphological properties of annealed silver film, the substrate was heated at various temperatures: 100, 125, 150, and 180 °C and held for 2, 5, 10, 15, and 20 min at each temperature.

Fig. 2 illustrates the variation in sheet resistance of the silver layer with annealing temperature, and hold time. The sheet resistance of the silver nanoparticle film was measured using four-point probe method. For comparison, sheet resistance of the evaporated silver film of 0.92 Ω sq^{-1} was used as a standard value. The silver nanoparticle film did not demonstrate a conductive behavior upon heating at 100 °C for over 20 min. It suggests that annealing temperature of ∼100 °C is the first stage of material transport (solvent evaporation) mechanism of nanoparticle silver inks. Upon increasing the annealing temperature to 125 °C for 2 min, the sheet resistance of the silver layer became ∼400 Ω sq^{-1} that suggested the initiation of the atomic diffusion stage. Upon further heating for 5 min, the sheet resistance plummeted dramatically and reached stabilized after 20 min at ∼13.2 Ω sq^{-1}. However, this value was still much higher than the standard value (0.92 Ω sq^{-1}). Upon further annealing at 180 °C for 5 min, the sheet resistance significantly decreased and stabilized itself at ∼0.35 Ω sq^{-1}. This rapid decline demonstrates that the silver nanoparticles were connected well to form a continuous and conductive network, as shown in Fig. 3. It is also evident from

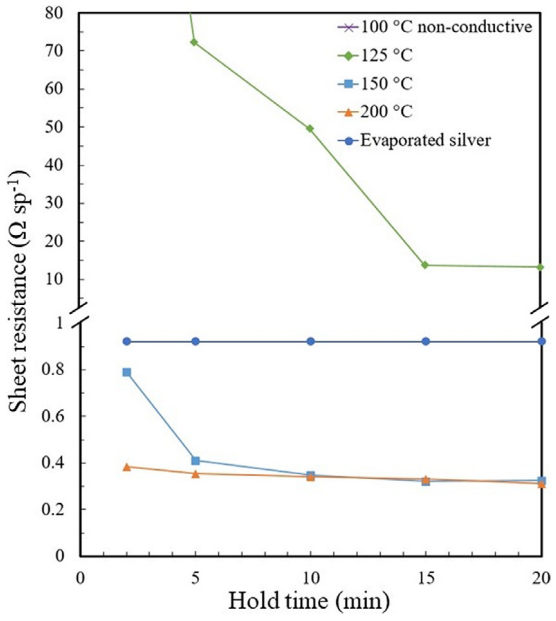

Fig. 2. Variation in sheet resistance of the silver layer with annealing temperature and hold time.

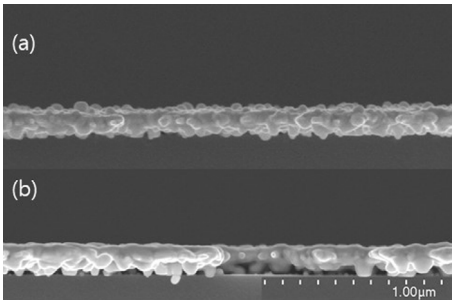

Fig. 3. The microstructure of silver nanoparticle film annealed at (a) 150 °C and (b) 180 °C for 5 min.

Fig. 3 that the microstructure of silver nanoparticle film is more dense at high temperature than at low temperature. However, the adhesion between silver nanoparticle film and the substrate become weaker because of the hole formation at the interface. The holes reduced the overall contact area at the interface and the silver nanoparticle film was easily peeled off. This problem might have risen because of fast evaporation of solvent in the nanoparticle silver inks at elevated temperatures. From these estimations, the annealing temperature of 150 °C was used in further experiments.

Fig. 4 illustrates the AFM topography of surface of the silver nanoparticle film annealed at 150 °C with different hold time. The surface roughness affects the contact area between top and bottom parts in lamination process. The AFM topographic measurements indicated that root mean squared (rms) roughness increased with increasing hold time and became stable after 10 min. It may be because of silver nanoparticle film achieving a maximum densification possible after 10 min. Although the rms roughness of 2.93 nm after hold time of 2 min showed a good smooth surface, sheet resistance was double as compared with that of longer hold time (Fig. 2). At hold time of 5 min, both sheet resistance of 0.40 Ω sq^{-1} (reaching nearly the stable value of 0.32 Ω sq^{-1}) and rms roughness of 4.09 nm provided a fairly good top electrode for the lamination process, and hence selected for further experiments. The silver nanoparticle film annealed at 150 °C for 5 min on PET substrate looks like a mirror, as described in Fig. 4(f).

A ∼1000-nm-thick PEDOT:PSS/D-sorbitol layer was prepared on the silver layer by spin-coating 100 μL of PEDOT:PSS/D-sorbitol solution at 1000 rpm for 60 s. This substrate was then annealed from 100 to 120 °C to eliminate water in pristine PEDOT:PSS and melt D-sorbitol (Nardes et al., 2008). However, the adhesion of PEDOT:PSS/D-sorbitol gradually decreases with an increase in annealing temperature. This is in accordance with the previous results (Makha et al., 2016). Hence, annealing temperature of 120 °C for 10 min was fixed and applied for further experiments.

Bases on the above estimation, we fabricated nice cells with lamination process as previously shown in Fig. 1(a). The laminated area of the cells was typically 1 × 1 cm^2 and masked

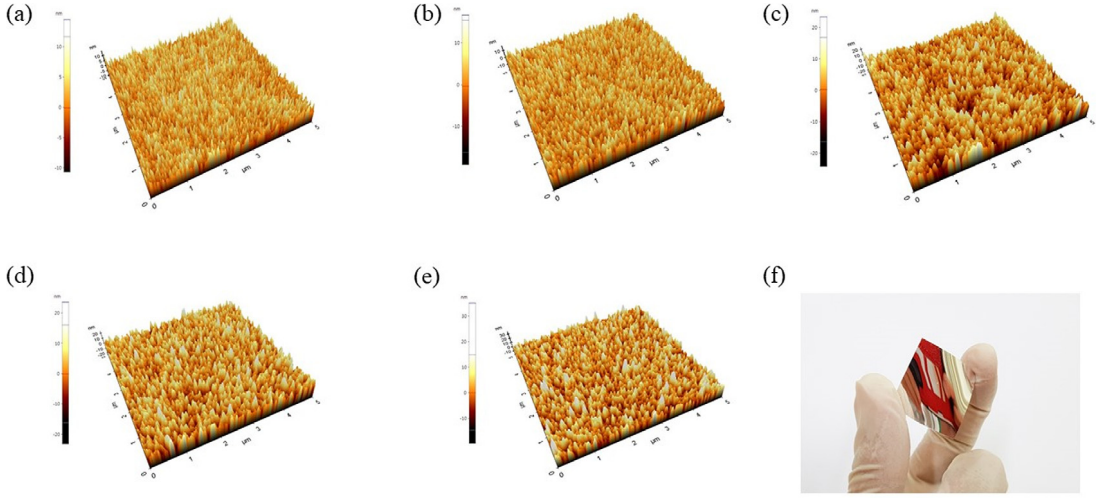

	2 min	5 min	10 min	15 min	20 min
Rms roughness	3.09	4.09	5.13	5.59	5.61

Fig. 4. The AFM topographic images of the surface of silver nanoparticle film annealed at 150 °C for different hold time: (a) 2 min, (b) 5 min, (c) 10 min, (d) 15 min, and (e) 20 min. (f) Silver nanoparticle film on a PET substrate.

Table 1
Average performance parameters of nine cells with conventional and laminated methods.

Configuration	Scan direction	V_{OC} (V)	J_{SC} (mA cm^{-2})	FF	PCE (%)
Conventional cells	Forward	0.97 ± 0.04	20.1 ± 0.65	0.54 ± 0.02	10.63 ± 0.67
	Backward	0.98 ± 0.03	19.3 ± 0.81	0.64 ± 0.02	11.19 ± 0.43
Laminated cells	Forward	0.96 ± 0.02	20.57 ± 0.75	0.43 ± 0.04	8.63 ± 0.63
	Backward	0.97 ± 0.02	16.96 ± 1.19	0.59 ± 0.03	10.03 ± 0.53

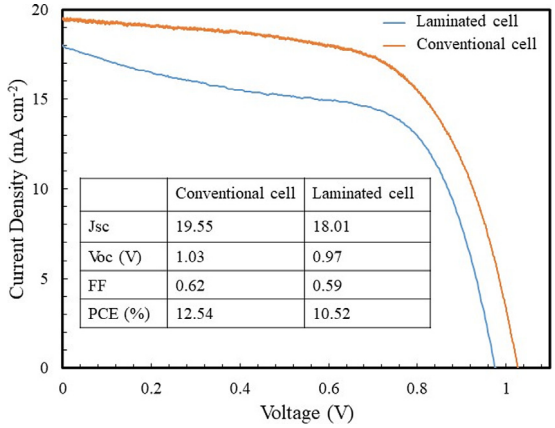

Fig. 5. J-V curve of the best performing cells measured by the backward scan at AM 1.5G one sun illumination.

with an aperture of diameter 5 cm to define the active area. To compare and evaluate the efficiency of laminated cells, nine conventional cells were produced using thermal evaporator. Table 1 and Fig. 5 show the average performance parameters of nine cells with conventional and laminated methods and J-V curves of the best performing cells, respectively. These parameters were achieved from 100% fabricated cells meaning that lamination process was perfectly trusted and the silver nanoparticle film worked properly as conventional silver electrode function: holes collection and reflection of non-absorbed light back into the active area. The J-V hysteresis with sweep direction was observed during measurement process in both types of solar cells, as described in Table 1. The average PCE with backward scan direction is higher than that of forward scan direction. This hysteresis is one of current issues of PSCs (Snaith et al., 2014). The data in Table 1 also indicate that the PCE of the laminated cells (10.03%) is slightly lower than that of conventional cells (11.19%), mainly due to lower FF and J_{SC}. The decrease in FF might be ascribed to the increase in series resistance from the addition of the PEDOT:PSS/D-sorbitol layer. Meanwhile, the poorer interfacial contact at hole-transport layer/laminated top electrode compared to the conventional method reduces the p-type charge collection leading to the lower J_{SC}.

Fig. 6 shows long-term stability of the PSCs. In this study, we used two of the best performance cells as the representatives of both types of perovskite solar cells. They were investigated for 28 days and measured every 7 days. Devices were kept in dark place with relative humidity from 35% to 50%. The PCE of conventional cell reduced steadily and remained about 75% of the initial PCE after 28 days, while the laminated cells dropped quickly after 7 days and remained only 15% of its initial PCE at the end of experiment day. The FF of the laminated cell was the fastest and the highest decline parameter. After 7 days, it reduced by 20% and remained only 32% of its initial FF after 28 days. The hygroscopic property of PEDOT:PSS can cause degradation of humidity sensitive components such as Spiro-MeOTAD and connection between two parts of laminated cell; hence performance parameters were strongly decreased. This was evident that laminated cells must be fabricated carefully and protected against moisture to increase the lifetime of the solar cell. Table 2 illustrates the photovoltaic parameters of the best cells at the start and at the end of the study.

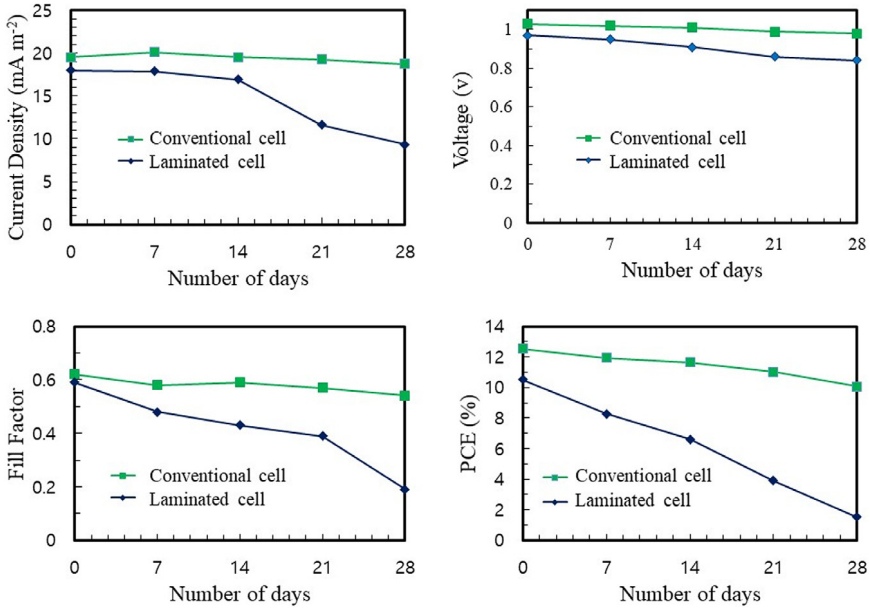

Fig. 6. Photovoltaic parameters of the best cells during the study of long-term stability.

Table 2
J-V parameters of the best cells before and after 28 days.

Configuration		V_{OC} (V)	J_{SC} (mA cm^{-2})	FF	PCE (%)
Conventional cells	First day	1.03	19.55	0.62	12.54
	After 28 days	0.98	18.74	0.54	10.06
Laminated cells	First day	0.97	18.01	0.59	10.52
	After 28 days	0.84	9.35	0.19	1.52

4. Conclusions

We presented a fully solution-processed method to fabricate perovskite solar cells, in which the silver nanoparticle film and PEDOT:PSS/D-sorbitol layer act as the top electrode and conductive adhesive, respectively. The silver nanoparticle film was easily created by spin-coating method and used as an alternative to the evaporated silver contact. It also exhibited an excellent conductivity and low surface roughness, which were desirable for lamination process. The perovskite solar cells were entirely fabricated under ambient conditions. This provided a simple and low-cost process and yet capable of achieving expected results. Our results indicate that the laminated cells show an average PCE of 10.03% reaching nearly that of conventional cells (11.19%). Although these cells are highly sensitive to humidity, yet they enable facile fabrication of perovskite solar cells.

CRediT authorship contribution statement

Xuan-Long Trinh: Conceptualization, Methodology, Writing - review & editing. **Hyun-Chul Kim:** Supervision, Conceptualization.

Declaration of competing interest

The authors declare that they have no known competing financial interests or personal relationships that could have appeared to influence the work reported in this paper.

Acknowledgments

This research was supported by Basic Science Research Program through the National Research Foundation of Korea (NRF) funded by the Ministry of Education (2017R1D1A1B03029074 and 2020054315).

References

Ball, J.M., Lee, M.M., Hey, A., Snaith, H.J., 2013. Low-temperature processed meso-superstructured to thin-film perovskite solar cells. Energy Environ. Sci. 6, 1739–1743. http://dx.doi.org/10.1039/c3ee40810h.

Best Research-Cell Efficiency Chart | Photovoltaic Research | NREL [WWW Document], n.d. URL https://www.nrel.gov/pv/cell-efficiency.html (accessed 8.13.19).

Bryant, D., Greenwood, P., Troughton, J., Wijdekop, M., Carnie, M., Davies, M., Wojciechowski, K., Snaith, H.J., Watson, T., Worsley, D., 2014. A transparent conductive adhesive laminate electrode for high-efficiency organic–inorganic lead halide perovskite solar cells. Adv. Mater. 26, 7499–7504. http://dx.doi.org/10.1002/adma.201403939.

Bu, L., Liu, Z., Zhang, M., Li, W., Zhu, A., Cai, F., Zhao, Z., Zhou, Y., 2015. Semitransparent fully air processed Perovskite solar cells. ACS Appl. Mater. Interfaces 7, 17776–17781. http://dx.doi.org/10.1021/acsami.5b04040.

Burschka, J., Pellet, N., Moon, S.J., Humphry-Baker, R., Gao, P., Nazeeruddin, M.K., Grätzel, M., 2013. Sequential deposition as a route to high-performance perovskite-sensitized solar cells. Nature 499, 316–319. http://dx.doi.org/10.1038/nature12340.

Chen, W., Liu, T., Sun, X., Guo, F., Wang, Y., Shi, C., Ghadari, R., Kong, F., 2019. Facile synthesis of simple arylamine-substituted naphthalene derivatives as hole-transporting materials for efficient and stable perovskite solar cells. J. Power Sources 425, 87–93. http://dx.doi.org/10.1016/j.jpowsour.2019.03.050.

Frost, J.M., Butler, K.T., Brivio, F., Hendon, C.H., van Schilfgaarde, M., Walsh, A., 2014. Atomistic origins of high-performance in hybrid Halide Perovskite solar cells. Nano Lett. 14, 2584–2590. http://dx.doi.org/10.1021/nl500390f.

Gaynor, W., Lee, J.Y., Peumans, P., 2010. Fully solution-processed inverted polymer solar cells with laminated nanowire electrodes. ACS Nano 4, 30–34. http://dx.doi.org/10.1021/nn900758e.

Giordano, F., Abate, A., Correa Baena, J.P., Saliba, M., Matsui, T., Im, S.H., Zakeeruddin, S.M., Nazeeruddin, M.K., Hagfeldt, A., Graetzel, M., 2016. Enhanced electronic properties in mesoporous TiO2 via lithium doping for high-efficiency perovskite solar cells. Nature Commun. 7, 10379. http://dx.doi.org/10.1038/ncomms10379.

Granström, M., Petritsch, K., Arias, A.C., Lux, A., Andersson, M.R., Friend, R.H., 1998. Laminated fabrication of polymeric photovoltaic diodes. Nature 395, 257–260. http://dx.doi.org/10.1038/26183.

Greer, J.R., Street, R.A., 2007. Thermal cure effects on electrical performance of nanoparticle silver inks. Acta Mater. 55, 6345–6349. http://dx.doi.org/10.1016/j.actamat.2007.07.040.

Guo, F., Azimi, H., Hou, Y., Przybilla, T., Hu, M., Bronnbauer, C., Langner, S., Spiecker, E., Forberich, K., Brabec, C.J., 2015. High-performance semitransparent perovskite solar cells with solution-processed silver nanowires as top electrodes. Nanoscale 7, 1642–1649. http://dx.doi.org/10.1039/C4NR06033D.

Huang, J., Li, G., Yang, Y., 2008. A semi-transparent plastic solar cell fabricated by a lamination process. Adv. Mater. 20, 415–419. http://dx.doi.org/10.1002/adma.200701101.

Hwang, H., Kim, A., Zhong, Z., Kwon, H.-C., Jeong, S., Moon, J., 2016. Reducible-shell-derived pure-copper-nanowire network and its application to transparent conducting electrodes. Adv. Funct. Mater. 26, 6545–6554. http://dx.doi.org/10.1002/adfm.201602094.

Im, J.H., Jang, I.H., Pellet, N., Grätzel, M., Park, N.G., 2014. Growth of CH3NH3PbI3cuboids with controlled size for high-efficiency perovskite solar cells. Nat. Nanotechnol. 9, 927–932. http://dx.doi.org/10.1038/nnano.2014.181.

Khaligh, H.H., Goldthorpe, I.A., 2013. Failure of silver nanowire transparent electrodes under current flow. Nanoscale Res. Lett. 8, 235. http://dx.doi.org/10.1186/1556-276X-8-235.

Kim, H.B., Choi, H., Jeong, J., Kim, S., Walker, B., Song, S., Kim, J.Y., 2014. Mixed solvents for the optimization of morphology in solution-processed, inverted-type perovskite/fullerene hybrid solar cells. Nanoscale 6, 6679–6683. http://dx.doi.org/10.1039/c4nr00130c.

Kim, H.-S., Lee, C.-R., Im, J.-H., Lee, K.-B., Moehl, T., Marchioro, A., Moon, S.-J., Humphry-Baker, R., Yum, J.-H., Moser, J.E., Grätzel, M., Park, N.-G., 2012a. Lead iodide perovskite sensitized all-solid-state submicron thin film mesoscopic solar cell with efficiency exceeding 9%. Sci. Rep. 2, 591. http://dx.doi.org/10.1038/srep00591.

Kim, Y.H., Müller-Meskamp, L., Zakhidov, Alexander A., Sachse, C., Meiss, J., Bikova, J., Cook, A., Zakhidov, Anvar A., Leo, K., 2012b. Semi-transparent small molecule organic solar cells with laminated free-standing carbon nanotube top electrodes. Sol. Energy Mater. Sol. Cells 96, 244–250. http://dx.doi.org/10.1016/J.SOLMAT.2011.10.001.

Kojima, A., Teshima, K., Shirai, Y., Miyasaka, T., 2009. Organometal halide perovskites as visible-light sensitizers for photovoltaic cells. J. Am. Chem. Soc. 131, 6050–6051. http://dx.doi.org/10.1021/ja809598r.

Liu, D., Kelly, T.L., 2013. Perovskite solar cells with a planar heterojunction structure prepared using room-temperature solution processing techniques. Nat. Photonics 8, 133.

Makha, M., Fernandes, S.L., Jenatsch, S., Offermans, T., Schleuniger, J., Tisserant, J.-N., Véron, A.C., Hany, R., 2016. A transparent, solvent-free laminated top electrode for perovskite solar cells. Sci. Technol. Adv. Mater. 17, 260–266. http://dx.doi.org/10.1080/14686996.2016.1176512.

Nardes, A.M., Kemerink, M., de Kok, M.M., Vinken, E., Maturova, K., Janssen, R.A.J., 2008. Conductivity, work function, and environmental stability of PEDOT:PSS thin films treated with sorbitol. Org. Electron. 9, 727–734. http://dx.doi.org/10.1016/J.ORGEL.2008.05.006.

Ouyang, J., Yang, Y., 2006. Conducting polymer as transparent electric glue. Adv. Mater. 18, 2141–2144. http://dx.doi.org/10.1002/adma.200502475.

Schloemer, T.H., Christians, J.A., Luther, J.M., Sellinger, A., 2019. Doping strategies for small molecule organic hole-transport materials: impacts on perovskite solar cell performance and stability. Chem. Sci. 10, 1904–1935. http://dx.doi.org/10.1039/C8SC05284K.

Shimada, C., Shiratori, S., 2013. Viscous conductive glue layer in semitransparent polymer-based solar cells fabricated by a lamination process. ACS Appl. Mater. Interfaces 5, 11087–11092. http://dx.doi.org/10.1021/am402698x.

Snaith, H.J., Abate, A., Ball, J.M., Eperon, G.E., Leijtens, T., Noel, N.K., Stranks, S.D., Wang, J.T.-W., Wojciechowski, K., Zhang, W., 2014. Anomalous hysteresis in perovskite solar cells. J. Phys. Chem. Lett 5, 1511–1515. http://dx.doi.org/10.1021/jz500113x.

Song, Z., Watthage, S.C., Phillips, A.B., Heben, M.J., 2016. Pathways toward high-performance perovskite solar cells: review of recent advances in organo-metal halide perovskites for photovoltaic applications. J. Photonics Energy 6, 022001. http://dx.doi.org/10.1117/1.jpe.6.022001.

Stranks, S.D., Snaith, H.J., 2015. Metal-halide perovskites for photovoltaic and light-emitting devices. Nat. Nanotechnol. 10, 391–402. http://dx.doi.org/10.1038/nnano.2015.90.

Yin, L., Zhao, Z., Jiang, F., Li, Z., Xiong, S., Zhou, Y., 2014. PEDOT:PSS top electrode prepared by transfer lamination using plastic wrap as the transfer medium for organic solar cells. Org. Electron. Phys. Mater. Appl. 15, 2593–2598. http://dx.doi.org/10.1016/j.orgel.2014.07.028.

Yoo, Y.G., Park, J., Umh, H.N., Lee, S.Y., Bae, S., Kim, Y.H., Jerng, S.E., Kim, Y., Yi, J., 2019. Evaluating the environmental impact of the lead species in perovskite solar cells via environmental-fate modeling. J. Ind. Eng. Chem. 70, 453–461. http://dx.doi.org/10.1016/J.JIEC.2018.11.008.

You, P., Liu, Z., Tai, Q., Liu, S., Yan, F., 2015. Efficient semitransparent perovskite solar cells with graphene electrodes. Adv. Mater. 27, 3632–3638. http://dx.doi.org/10.1002/adma.201501145.